coatings

Article

Effects of Splat Interfaces, Monoclinic Phase and Grain Boundaries on the Thermal Conductivity of Plasma Sprayed Yttria-Stabilized Zirconia Coatings

Xiaojie Guo [1], Weiwei Zhao [1], Yi Zeng [1,2,*], Chucheng Lin [1] and Jimei Zhang [1]

[1] The State Key Lab of High Performance Ceramics and Superfine Microstructure, Shanghai Institute of Ceramics, Chinese Academy of Sciences, Shanghai 200050, China; guoxiaojie@mail.sic.ac.cn (X.G.); wwzhao1218@163.com (W.Z.); chucheng@mail.sic.ac.cn (C.L.); jmzhang@mail.sic.ac.cn (J.Z.)

[2] Center of Materials Science and Optoelectronics Engineering, University of Chinese Academy of Sciences, Beijing 100049, China

* Correspondence: zengyi@mail.sic.ac.cn; Tel.: +86-21-6916-3697

Received: 20 September 2018; Accepted: 27 December 2018; Published: 3 January 2019

Abstract: Microstructure has a significant influence on the thermal conductivity of thermal barrier coating (TBC) systems. In this work, the microstructures including splat interface, monoclinic phase and grain boundaries in the YSZ air plasma spraying (APS) TBC systems are investigated. A finite element simulation model based on electron backscatter diffraction (EBSD) images is established. It is found that the simulation results of thermal conductivity are in good agreement with the experimental results. Using this model, the effect coefficient of splat interface, monoclinic phase and grain boundaries on thermal conductivity are calculated. Results show that the splat interface influences the thermal conductivity of the TBCs. Those results provide important guidance for reducing the thermal conductivity of thermal barrier coatings.

Keywords: YSZ coatings; finite element models; EBSD images; thermal conductivity; microstructure

1. Introduction

Thermal barrier coatings (TBCs), an oxide ceramic layer for the protection of a substrate material, are widely used for the thermal, oxidation and hot corrosion protection of high-temperature components in gas turbines [1]. The coatings provide insulation to metallic structures, thus, delaying the thermally-induced failure that governs the component durability and life [2,3]. However, as the thrust–weight ratio of engines become higher, the temperature of gas turbines for military aircraft engines has reached 1700 °C. The operating temperature of traditional YSZ coatings is generally lower than 1200 °C, which cannot meet the requirements of future military aircraft engines [4,5]. Therefore, the method to reduce the thermal conductivity of YSZ coatings became a hot topic in recent years. The thermal conductivity of YSZ coatings is closely related to the microstructure; therefore, it is necessary to study the microstructure of the TBCs in order to reduce its thermal conductivity.

Numerous works have investigated the relationship between the microstructures and thermal conductivity. Pores and cracks are the most important factors affecting the thermal conductivity. Moreover, there have been many studies on the effect of pores and cracks that focus on thermal conductivity. Chi and coworkers used image analysis (IA) data to simulate the effect of porosity on the thermal diffusivity; it turns out a very fast increase in the thermal diffusivity within the first 15 h of service. It might be due to the crack-like pores that filled with air through this process and to the thermal diffusivity of air (2.2×10^{-5} m^2·s^{-1}) which is roughly two orders of magnitude higher than the air thermal diffusivity of typical YSZ porous TBCs ($3–5 \times 10^{-7}$ m^2·s^{-1}) [6]. Chi et al. [7] compared coatings with different microstructures prepared with different feedstocks and different spraying processes, then analyzed structure–thermal conductivity images during thermal cycling. The results revealed that more interface, higher porosity and more interlamellar pores can reduce the thermal conductivity of TBCs. Increasing the length and width of the interlamellar pores at high temperatures can reduce the tendency of the coating to sinter, thereby lowering the thermal conductivity of TBCs. However, no quantitative relationship was provided between the microstructure and thermal conductivity.

Wei and coworkers quantified the influence of pore radius and crack length on effective thermal conductivity. It is found that the longest crack has the greatest effect on thermal conductivity [8]. Clyne and Golosnoy established equations of pores to predict thermal conductivity of TBCs using Eshelby-based and contact-based analytical models respectively [9,10]. When the Eshelby-based model is used in materials with high porosity, the calculated results are found to be higher than the experimental results because the Eshelby-based analytical model depends upon the assumption that only the tetragonal phase is present. Contact-based analysis models have been adopted to predict the microstructure changes during sintering. However, the establishment of these models is based on the analysis of SEM images, leading to the establishment of an equation that is roughly similar to the experimental value rather than based on the actual microstructure and resulting in the limitations of model application. To research the relationship between interface and thermal conductivity, the model of heat conduction established by McPherson [11], the model of object oriented finite (OFF) established by Wang et al. [12] and the mathematical formula that can calculate the influence of the interface on thermal conductivity established by Wei and his colleagues [13] all made explanations for low thermal conductivity of the coatings with the lamellae. They think that the lamellar interspaces are equivalent to the pores parallel to the interface and that the width of the pores is equivalent to the average free path of the gas molecules, which limits the conduction of heat flow. In these studies, the influence of the splat interface on the coating performance was quantified and the influence coefficient was calculated to account for 25%–70% of the total influence, but the establishment of these model is also based on SEM microstructure observations followed by simulation calculations, which fail to calculate based on the true microstructure the influence coefficients of the grain boundaries, interface and monoclinic separately.

Therefore, we tried to establish a finite element (FE) model based on the microstructure of electron backscatter diffraction (EBSD) analysis because more information, such as grain size and phase composition, can be easily obtained by EBSD compared with SEM. Hence, it is more accurate to establish the FE model based on EBSD images when we consider the influence of multiple factors on the thermal conductivity. The effect coefficient of grain boundaries, interfaces and monoclinic phase on thermal conductivity are directly calculated; additionally, it provides a reference for how to guide the spraying process to lower the thermal conductivity of the coatings.

2. Materials and Methods

Commercially-available ZrO_2-3% mol Y_2O_3 nanopowder and micropowder were used. Metco A-2000 APS equipment was used to deposit the coatings onto aluminum substrates (Guan Yu special Alloy products Co. Ltd., Shanghai, China, 128 mm × 84 mm × 2 mm). Two specimens, designated as M_1 and M_2, were sprayed with nanopowder. A third specimen, designated as M_3, was sprayed with micropowder. The spray gun parameters are listed in Table 1.

Table 1. The spraying parameters.

Sample \ Parameters	Current (A)	Voltage (V)	Primary Plasma Gas (Ar)	Secondary Plasma Gas (H_2)	Feed Rate ($g{\cdot}min^{-1}$)	Spray Distance (mm)
M_1	560	68	25	12	25	120
M_2	600	69	25	12	30	130
M_3	500	62	40	7	25	120

Microstructure of the YSZ coating is characterized by SEM (Magellan 400, FEI, Hillsboro, OR, USA) equipped with an EBSD detector. EBSD provides the conditions for the analysis of crystal microdomain orientation and crystal structure while preserving the conventional features of SEM. Through EBSD image analysis of a certain sample area, the size, distribution, orientation and grain boundary distribution of the crystal grains and the phase contained in the area can be obtained.

In this study, 25 EBSD images were selected for each YSZ coating, and an FE mesh model that is consistent with the true microstructure is generated. The FE meshes of the M_1, M_2 and M_3 coatings with microstructures are illustrated in next part. The thermal conductivities of the YSZ coatings are obtained through a steady-state heat transfer analysis, while the thermal conductivity of ceramics in the direction of the temperature gradient can be computed with Fourier's equation:

$$\lambda = \lambda_{\mathrm{m}} \frac{h \cdot \int_{\Gamma} \nabla T \, \mathrm{d}\, \Gamma}{l \cdot \nabla T} \tag{1}$$

where h is the thickness of ceramic, l is the width, λ_{m} represents the thermal conductivity for the bulk material, Γ is the integral path of the heat flux density and ∇T is the temperature gradient.

The thermal conductivity of the tetragonal phase, the grain boundaries and the splat interface are 2.65, 1.54 and 0.03 W/m·K, respectively [14]. Rhagavan et al. revealed that the thermal conductivity of pure monoclinic zirconia with 98% density was 3.6 W/m·K [15]. Thus, the thermal conductivity of monoclinic phase in our model is also set to be 3.6 W/m·K. The thermal conductivity of each content is shown in Table 2.

Table 2. The thermal conductivity input data.

Content	Thermal Conductivity (W/m·K)
tetragonal phase	2.65
grain boundaries	1.54
splat interface	0.03
monoclinic phase	3.60

3. Results and Discussion

3.1. The Microstructure of YSZ Coatings

The EBSD images of the polished cross-sections of the YSZ thermal barrier coatings and the cross-section backscattered image of M_3 are shown in Figure 1. The phase composition of each sample and the content of each phase, the distribution of cracks, the pores and the grain boundaries can be observed from the EBSD images. Different colors indicate different compositions. Red represents the monoclinic phase, green represents tetragonal phase, black represents grain boundaries and white represents cracks and pores. In the process of APS, the spraying powers for the coatings of M_1 and M_3 were lower than that of coating M_2. This caused the lower temperatures of in-flight particles in as-sprayed M_1 and M_3 coatings and then led to worse melting state. Therefore, the porosities of coatings M_1 and M_3 were higher compared with that of coating M_2. Furthermore, the larger raw spraying powders for coating M_3 also contributed to the relatively worse melting of in-flight particles, which resulted in more pores in the coating M_3. The content of monoclinic phase, tetragonal phase, cracks and pores can be obtained from the data measured by EBSD; all are listed in Table 3.

Table 3. Microstructures parameters.

Coating	Monoclinic Phase (%)	Pores and Cracks (%)	Tetragonal Phase (%)	Grain Boundary Densities (m/μm^2)	The Average Grain Size (nm)
M_1	1.91	15.98	82.11	2.51	980
M_2	2.13	13.01	84.86	2.23	1200
M_3	8.02	30.02	61.96	1.48	1620

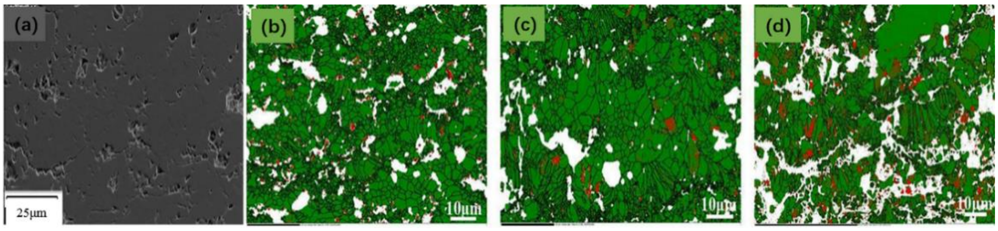

Figure 1. Cross-section backscattered image of (**a**) M_3, and the EBSD images of polished cross-sections of the YSZ thermal barrier coatings (**b**) M_1, (**c**) M_2 and (**d**) M_3.

3.2. Simulation of Thermal Conductivity

The FE meshes of the M_1, M_2 and M_3 coatings with varied microstructures are illustrated in Figure 2a–c, respectively. The thermal conductivity of the coating along the spray direction is calculated. The distributions of the thermal gradient along the spray direction under steady-state conditions are shown in Figure 3a–c, and the thermal fluxes are shown in Figure 3d–f, pertaining to coatings M_1, M_2 and M_3, respectively. The simulation results λ_s and experimental results λ_0 of thermal conductivity are listed in Table 4.

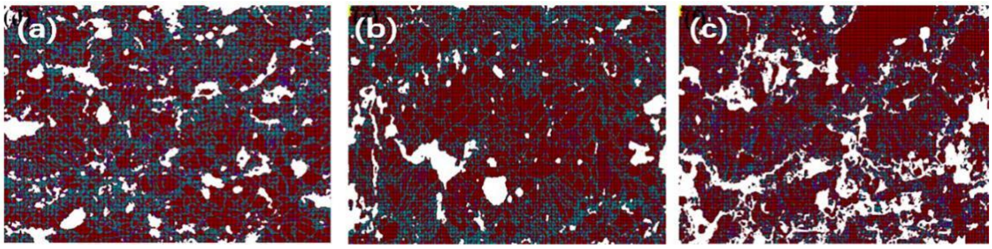

Figure 2. The finite element mesh (**a**) M_1, (**b**) M_2 and (**c**) M_3.

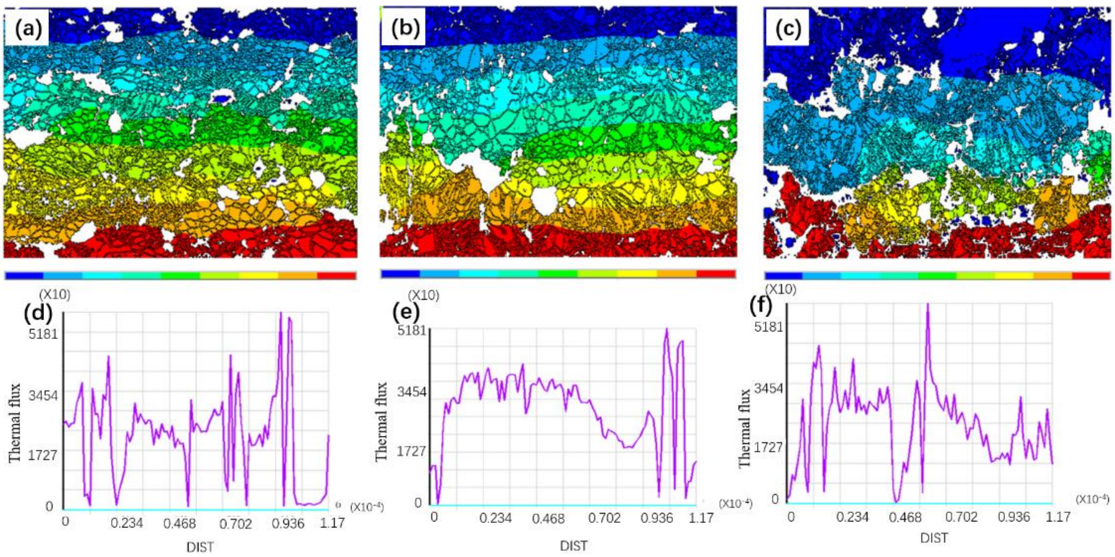

Figure 3. Distributions of thermal gradient (**a**) M_1, (**b**) M_2 and (**c**) M_3, and the thermal flux of coatings: (**d**) M_1, (**e**) M_2 and (**f**) M_3.

Table 4. The comparison of theoretical results λs and experimental results λ_0.

Coating	The Simulation Results λs (W/m·k)	Experimental Findings λ_0 (W/m·k)	Calculation Errors (%)
M_1	1.76	1.244	41.48
M_2	1.9	1.29	47.29
M_3	1.55	1.27	22.05

Comparisons show that the calculation error is very large because the splat interfaces cannot be seen in the EBSD image. However, the splat interfaces have a significant influence on the thermal conductivity of YSZ coatings [11]. This influence will be discussed later in detail.

3.3. The Effect of Splat Interface on the Thermal Conductivity

To analyze the effect of the splat interfaces on thermal conductivity, an idealized model was introduced. In a study by Shen et al. [13], an artificial image with dimensions of 25 μm × 25 μm was created, and all the splat interfaces were represented as rectangular elements having a size of 3.25 μm × 0.125 μm, as indicated in Figure 4. The thermal conductivity of splat interfaces is obtained through iterative computation and was set to 0.03 W/m·K, which made the simulated thermal conductivities map well with the experimental thermal conductivities of as-sprayed coatings [16]. The distribution of the thermal flux about the coating is shown in Figure 5. Using Equation (1), the thermal conductivities of the coatings were calculated. The simulation results (λ_c) and the experimental findings (λ_0) are listed in Table 5.

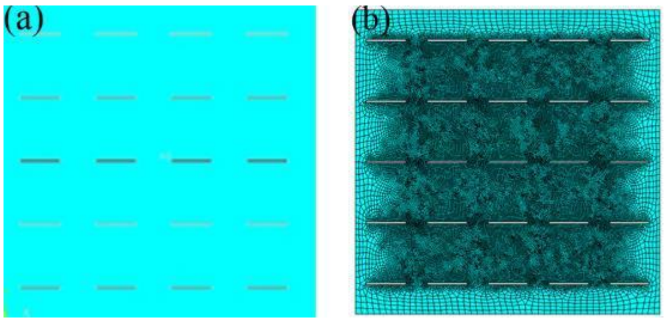

Figure 4. (**a**) An idealized model of YSZ coatings; (**b**) finite element mesh of the idealized model.

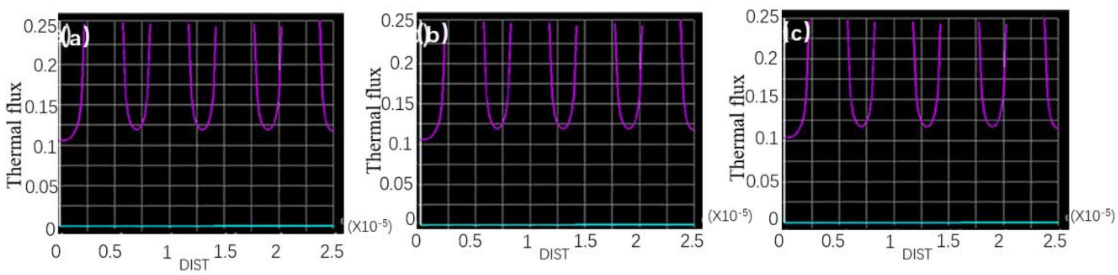

Figure 5. The distributions of thermal flux about the coatings (**a**) M_1, (**b**) M_2 and (**c**) M_3.

Table 5. Comparison of theoretical and experimental results.

Coating	Simulation Result λ_c (W/m·k)	Experimental Findings λ_0 (W/m·k)	Calculation Errors (%)
M_1	1.28	1.244	2.9
M_2	1.38	1.29	6.98
M_3	1.16	1.27	8.66

The phase composition and content of grain boundaries were easily obtained through the EBSD image as shown in Figure 1. Furthermore, when the ideal splat interface model was introduced, the simulated thermal conductivity and experimental thermal conductivity can be matched well. Therefore, it is more accurate to use this model to figure out the influence coefficient of thermal conductivity for the splat interface, grain boundaries and monoclinic phase. The thermal conductivity of pores and cracks, tetragonal phase, monoclinic phase, grain boundaries and splat interface were placed in the simulation model. The thermal fluxes of coatings without splat interface is obtained based on the finite element mesh in Figure 2 and is represented in Figure 6. The distribution of the thermal gradient and thermal flux under steady-state conditions can be estimated through the FE grid and are shown in Figure 7. By combining the results with Equation (1) and (2), the thermal conductivity λ_1 of the coating with splat interface and λ_2 without splat interface, the change in the thermal conductivity ($\Delta\lambda_1$) under the influence of the splat interface and the effect coefficient R_2 obtained are therefore listed in Table 6.

$$R_1 = \frac{\lambda_1 - \lambda_2}{\lambda_0} \times 100\% \tag{2}$$

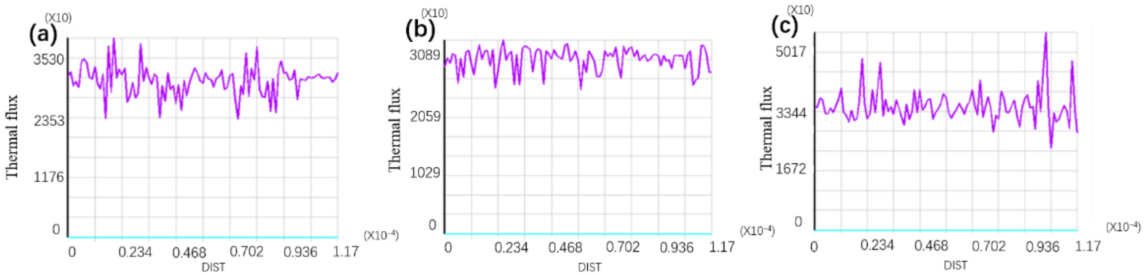

Figure 6. Thermal flux of coatings without splat interface (**a**) M_1, (**b**) M_2 and (**c**) M_3.

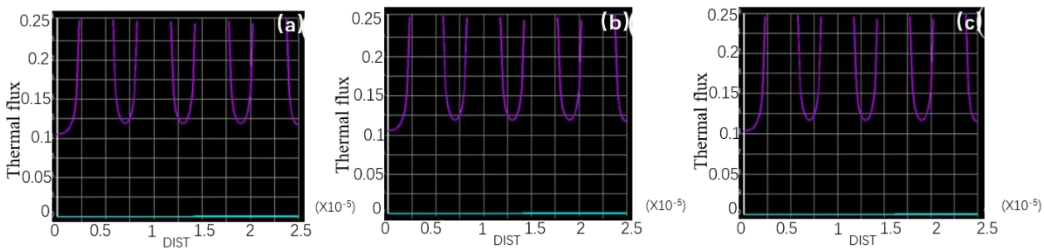

Figure 7. Thermal flux of coatings with splat interface (**a**) M_1, (**b**) M_2 and (**c**) M_3.

Table 6. The simulation results λ_1, λ_2, the effect coefficient R_1.

Coating	The Simulation Result of Coatings without Interface λ_1 (W/m·k)	The Simulation Result of Coatings with Interface λ_2 (W/m·k)	Change of Thermal Conductivity $\Delta\lambda_1$ (W/m·k)	The Effect Coefficient of Splat Interface R_1 (%)
M_1	2.46	1.8	−0.66	53.1
M_2	2.474	1.83	−0.64	49.9
M_3	2.798	2.1	−0.70	54.9

It can be concluded that the splat interfaces have a significant influence on the decrease of thermal conductivity of YSZ TBCs, and the effect coefficient can reach 50%. The reason is that the splat interface can cause phonon scattering and reduce the phonon mean free path. Furthermore, the lamellar spaces are similar to the pores parallel to the interface, and the pores will cause further phonon scattering, making great reduction of the heat transfer ability of the coatings.

On the basis of Tables 5–7, it could be found that the order of experimental thermal conductivity is $M_1 < M_3 < M_2$. However, the order of simulated thermal conductivity is different, in which the M_3 shows the maximum thermal conductivity. It is probably attributed to the fact that the same idealized splat interface models were introduced in all three coatings. In fact, the splat interfaces should also be different from each other due to the differences of the microstructures for the three coatings, as shown in EBSD and SEM images. Therefore, it inevitably leads to different deviation levels in the as-simulated thermal conductivity and finally results in the different trends of simulated and experimental thermal conductivities. It might be one of the major limitations of this model.

Table 7. The simulation results λ_m, λ_3 and the effect coefficient R_2.

Coating	Simulation Results of Coatings without Monoclinic Phase λ_m (W/m·k)	Simulation Result of Coatings with Monoclinic Phase λ_3 (W/m·k)	Change of Thermal Conductivity $\Delta\lambda_2$ (W/m·k)	Effect Coefficient of Monoclinic Phase R_2 (%)
M_1	2.37	2.46	0.09	7.23
M_2	2.4	2.474	0.07	5.43
M_3	2.51	2.798	0.288	22.68

3.4. The Effect of Monoclinic Phase on the Thermal Conductivity

To elucidate the effect of the monoclinic phase on the thermal conductivity, the thermal conductivity (λ_3) of the coating with monoclinic phase, tetragonal phase, grain boundaries and splat interface are compared with the thermal conductivity (λ_m) of a coating that contains tetragonal phase, grain boundaries and splat interface. According to the idealized FE model, the pores, cracks and monoclinic phase are regarded as the tetragonal phase. Thus, the distributions of the thermal gradient and thermal flux under steady-state condition of the TBCs without monoclinic phase can be obtained, as listed in Figure 8. Similarly, when only cracks and pores are regarded as the tetragonal phase, the distributions of the thermal gradient and thermal flux under steady-state condition of the TBCs with monoclinic phase can be obtained, and it was indicated in Figure 9. Using Equation (1) along with these results, λ_m and λ_3 can be calculated, as listed in Table 6. The effect coefficient of the monoclinic phase R_2 on the thermal conductivity of the coating and the change in thermal conductivity $\Delta\lambda_2$ can be evaluated according to Equation (3).

$$R_2 = \frac{\lambda_3 - \lambda_m}{\lambda_0} \times 100\% \quad (3)$$

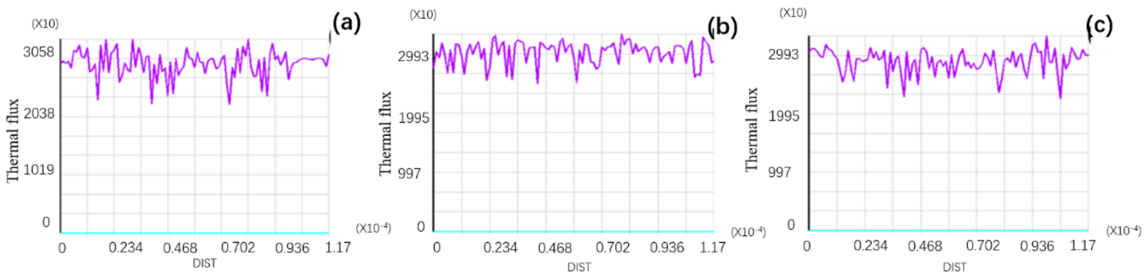

Figure 8. Distributions of thermal flux on the materials without monoclinic phase (**a**) M_1, (**b**) M_2 and (**c**) M_3.

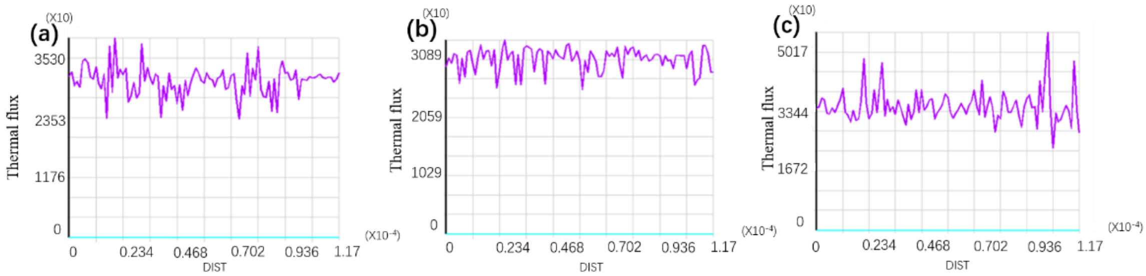

Figure 9. Distributions of thermal flux on the materials with monoclinic phase (**a**) M_1, (**b**) M_2 and (**c**) M_3.

The amount of monoclinic phase in each coating is listed in Table 3. The monoclinic phase has a very small concentration of 2% in coatings M_1 and M_2, and the thermal conductivity of the coating is increased by 0.1 W/m·K correspondingly according to Table 7. Furthermore, comparing M_2 with M_3 when the concentration of the monoclinic phase is increased by 6%, the value of the thermal conductivity with monoclinic phase increased by 0.28 W/m·K. Thus, it can be concluded that the monoclinic phase can increase the thermal conductivity of the coatings. The reason is that the content of Y^{3+} in the monoclinic YSZ decreased, leading to the reduction of point defects and lattice distortions. As a result, the scattering ability of the microstructure for phonons decreases, resulting in an increase in the phonon mean free path. In order to get a coating with a very low thermal conductivity, the content of the monoclinic phase should be kept at minimum.

In our study, the simulation results indicate that thermal conductivity of as-sprayed YSZ coatings at room temperature reduces with the decrease in the content of monoclinic phase. Therefore, the monoclinic phase should be avoided during practical spraying processes to reduce the thermal conductivity of YSZ coatings, which is consistent with the previous researches [17] and common practices. After thermal cycles, the content of monoclinic phase does increase because YSZ coatings would undergo a martensitic phase transformation from tetragonal zirconia to monoclinic zirconia at temperatures above 1200 °C. To avoid the increase of the content of monoclinic phase after thermal cycles, which would result in the increase of thermal conductivity at service temperature, the common practice solution is to improve the thermal stability of YSZ coatings. For example, the thermal stability of YSZ coatings could be improved, and the monoclinic phase was suppressed during thermal cycles by fabricating coatings of Al_2O_3 doped YSZ materials [18].

3.5. Effects of Grain Boundaries on the Thermal Conductivity

The thermal conductivity of the coatings λ_m that contain the tetragonal phase and grain boundaries can be seen in Table 6. The simulation results of the coatings for λ_m are compared with the thermal conductivity of the tetragonal phase, λ_T. The effect coefficient, R_3, of the grain boundaries on the thermal conductivity of the thermal spray coating can be obtained using Equation (4). Namely, the magnitude of the change in the thermal conductivity of the coatings via the grain boundary can also be calculated. The effect coefficient of the grain boundaries R_3 and the amount of change $\Delta\lambda_3$ are listed in Table 8.

$$R_3 = \frac{\lambda_m - \lambda_T}{\lambda_0} \times 100\% \tag{4}$$

Table 8. Effect coefficient of grain boundaries R_3 and the amount of change in thermal conductivity $\Delta\lambda_3$.

Coating	Thermal Conductivity of Tetragonal Phase λ_T (W/m·k)	Change of Thermal Conductivity $\Delta\lambda_3$ (W/m·k)	Effect Coefficient of the Grain Boundary R_3 (%)
M_1	2.65	−0.28	22.51
M_2	2.65	−0.25	19.38
M_3	2.65	−0.14	11.02

M_1 and M_2 are nanocoatings which were sprayed with nanopowders, while M_3 was sprayed with a micropowder. Thus, the different coatings have various grain sizes. Normally, when the grain size is reduced, the concentration of grain boundaries will be increased. The grain boundaries have the characteristic of phonon scattering and can reduce the phonon mean free path, leading to a reduction in the thermal conductivity of the coating. The effect coefficient of the grain boundaries is about 20% for each nanocoating. The grain boundaries play a vital role in the total reduction of the thermal conductivity.

4. Conclusions

The FE model was established based on EBSD analysis, which could offer more microstructure information. At the same time, an ideal interface model was introduced. The computational results are in agreement with the experimental findings, and the calculation error is lower than 10%. Using this model can simulate the effect of each microstructure on thermal conductivity more accurately.

The splat interface and grain boundaries play a critical role in the reduction of thermal conductivity, and the influence coefficient of the interface on thermal conductivity is much larger than that of the grain boundary. Therefore, it is necessary to take the splat interface into consideration when simulating the influence of microstructures on thermal conductivity. Moreover, when studying methods for reducing the thermal conductivity of coatings, the introduction of splat interfaces is a worthwhile consideration.

Author Contributions: Conceptualization, J.Z.; Formal Analysis, X.G. and W.Z.; Funding Acquisition, Y.Z.; Investigation, X.G.; Methodology, X.G., W.Z., C.L. and J.Z.; Project Administration, Y.Z.; Resources, Y.Z.; Software, C.L.; Writing-Original Draft, X.G.; Writing-Review and Editing, X.G.

Funding: This research was funded by National Key R & D program of China (No. 2018YFB0704400), International Partnership Program of Sciences (No. GJHZ1721), CAS key foundation for exploring scientific instrument (No. YJKYYQ20170041), Shanghai sailing program (No. 18YF1427000), Shanghai foundation for new research methods (No. 17142201500), Key Research Program of Frontier Science CAS, and Postdoctor industry base, Baoshan District Shanghai.

Acknowledgments: The authors are grateful for the technical assistance provided by Xuemei Song.

Conflicts of Interest: The authors declare no conflict of interest.

References

1. Goward, G.W. Progress in coatings for gas turbine airfoils. *Surf. Coat. Technol.* **1998**, *109*, 73–79. [CrossRef]
2. Nitin, P.P.; Maurice, G.; Eric, H.J. Thermal barrier coatings for gas-turbine engine applications. *Science* **2002**, *296*, 280–284. [CrossRef]
3. Sun, X.X.; Chen, H.F.; Yang, G.; Liu, B.; Gao, Y.F. YSZ-Ti_3AlC_2 thermal barrier coating and its self-healing behavior under high temperatures. *J. Inorg. Mater.* **2017**, *32*, 1269–1274. [CrossRef]
4. Li, C.J.; Ohmori, A. Relationships between the microstructure and properties of thermally-sprayed deposits. *J. Therm. Spray Technol.* **2002**, *11*, 365–374. [CrossRef]
5. Khor, K.A.; Gu, Y.W. Thermal properties of plasma-sprayed functionally graded thermal barrier coatings. *Thin Solid Films* **2000**, *372*, 104–113. [CrossRef]
6. Cernuschi, F.; Bison, P.G.; Marinetti, S.; Scardi, P. Thermophysical, mechanical and microstructural characterization of aged free-standing plasma-sprayed zirconia coatings. *Acta Mater.* **2008**, *56*, 4477–4488. [CrossRef]
7. Chi, W.; Sampath, S.; Wang, H. Microstructure-thermal conductivity relationships for plasma-sprayed yttria-stabilized zirconia coatings. *J. Am. Ceram. Soc.* **2008**, *91*, 2636–2645. [CrossRef]
8. Shen, W.; Wang, F.C.; Fan, Q.B.; Ma, Z. Effects of defects on the effective thermal conductivity of thermal barrier coatings. *Appl. Math. Model.* **2012**, *36*, 1995–2002. [CrossRef]
9. Clyne, T.W.; Golosnly, I.O.; Tan, J.C.; Markaki, A.E. Porous materials for thermal management under extreme conditions. *Philos. Trans. R. Soc. A* **2006**, *364*, 125–146. [CrossRef] [PubMed]
10. Golosnoy, I.O.; Tsipas, S.A.; Clyne, T.W. An analytical model for simulation of heat flow in plasma-sprayed thermal barrier coatings. *J. Therm. Spray Technol.* **2005**, *14*, 205–214. [CrossRef]

11. McPherson, R. A model for the thermal conductivity of plasma sparyed ceramic coatings. *Thin Solid Films* **1984**, *112*, 89–95. [CrossRef]
12. Wang, Z.; Kulkarni, A.; Deshpande, S.; Nakamura, T.; Herman, H. Effects of pores and interfaces on the effective properties of plasma sprayed zirconia coatings. *Acta Mater.* **2003**, *51*, 5319–5334. [CrossRef]
13. Shen, W.; Wang, F.C.; Fan, Q.B.; Hua, D.; Ma, Z. Proposal of new expressions for effects of splat interfaces and defects on effective properties of thermal barrier coatings. *Surf. Coat. Technol.* **2010**, *204*, 3376–3381. [CrossRef]
14. Zhao, W.W.; Chen, X.X.; Lin, C.C.; Song, X.M.; Zeng, Y.; Chang, C.K. quantitative calculation of thermal conductivity of tetragonal phase and grain boundary on zirconia ceramics. *J. Inorg. Mater.* **2017**, *11*, 1177–1180. [CrossRef]
15. Raghavan, S.; Wang, H.; Dinwiddie, R.B.; Porter, W.D.; Mayo, M.J. The effect of grain size, porosity and yttria content on the thermal conductivity of nanocrystalline zirconia. *Scr. Mater.* **1998**, *39*, 1119–1125. [CrossRef]
16. Lu, L.; Wang, F.C.; Ma, Z.; Fan, Q.B. Anisotropic effect of splat interface on thermal conductivity of plasma sprayed YSZ coating. *Surf. Coat. Technol.* **2013**, *235*, 596–602. [CrossRef]
17. Hu, N.N.; Khan, M.; Wang, Y.Z.; Song, X.M.; Lin, C.C.; Chang, C.K.; Zeng, Y. Effect of microstructure on the thermal conductivity of plasma sprayed Y_2O_3 stabilized Zirconia (8% YSZ). *Coatings* **2017**, *7*, 198. [CrossRef]
18. Song, X.M.; Liu, Z.W.; Kong, M.G.; Lin, C.C.; Huang, L.P.; Zheng, X.B.; Zeng, Y. Thermal stability of yttria-stabilized zirconia (YSZ) and YSZ-Al_2O_3 coatings. *Ceram. Int.* **2017**, *43*, 14321–14325. [CrossRef]